Geophysical Research Letters

RESEARCH LETTER
10.1029/2023GL103459

Majority of Southern Ocean Seasonal Sea Ice Zone Bloom Net Community Production Precedes Total Ice Retreat

S. McClish[1] **and S. M. Bushinsky**[1]

[1]Department of Oceanography, School of Ocean and Earth Science and Technology, University of Hawai'i at Mānoa, Honolulu, HI, USA

Key Points:

- The majority of net community production during the Southern Ocean seasonal sea ice zone bloom occurs prior to full sea ice retreat
- The highest rates of daily net community production occur during active sea ice retreat and may be due to iron delivery or low grazing rates
- Bloom net community production is higher in seasons where floats observe early sea ice retreat and/or are near topographic features

Supporting Information:

Supporting Information may be found in the online version of this article.

Correspondence to:

S. McClish,
smcclish@hawaii.edu

Citation:

McClish, S., & Bushinsky, S. M. (2023). Majority of Southern Ocean seasonal sea ice zone bloom net community production precedes total ice retreat. *Geophysical Research Letters*, *50*, e2023GL103459. https://doi.org/10.1029/2023GL103459

Received 6 MAR 2023
Accepted 11 SEP 2023

Abstract The Southern Ocean seasonal sea ice zone (SIZ) spring is characterized by sea ice retreat and the development of phytoplankton blooms. Until recently, assessing SIZ blooms and associated net community production (bNCP) has been limited by a lack of under-ice observations. We relate the timing of phytoplankton growth to the drawdown of surface nitrate and sea ice cover and estimate bNCP from biogeochemical profiling float observations. The onset of biological production closely follows initial sea ice breakup and, on average, 64% of bNCP occurs before total sea ice retreat. This indicates that satellite-derived estimates largely miss under-ice production and underestimate SIZ bNCP. Float bNCP estimates range from <1 to >4 mol C m^{-2} $bloom^{-1}$, with higher bNCP when sea ice breakup occurs early in the year, and the highest bNCP near topographic features that may increase micronutrient supply. Our results suggest changes in Southern Ocean sea ice will influence future bNCP.

Plain Language Summary Sea ice around the Southern Ocean expands during the fall/winter and retreats each spring/summer. Massive phytoplankton blooms are observed in recently ice-free waters, but observations of these blooms under-ice have previously been limited due to sampling challenges including rough winter seas and sea ice cover. This has made quantification of their ecological impact difficult. In this study we use year-round data from profiling floats that measure temperature, salinity, oxygen, nitrate, chlorophyll fluorescence, and particulate backscatter. We determine that phytoplankton growth begins after sea ice first begins to break up. The majority of organic matter that is produced but not consumed during the bloom is generated before total sea ice retreat. This indicates that commonly used satellite observations, which are blocked by sea ice, miss most of the bloom period. We also found the greatest net organic matter production when sea ice breakup occurred early in the season or near oceanic ridges and islands. We suggest phytoplankton growth limitation by micronutrients and consumption by grazers may contribute to the seasonal changes in organic matter production identified in this study. These results suggest that changes in sea ice timing and extent due to climate change will likely impact Southern Ocean biological production.

1. Introduction

The seasonal sea ice zone (SIZ) encompasses the roughly 16 million km^2 Southern Ocean region between the winter maximum and summer minimum sea ice extent. Winter sea ice formation inhibits air-sea gas exchange and deepens the surface mixed layer through cooling and brine rejection (Pellichero et al., 2017). In spring, sea ice rapidly retreats and freshens the surface ocean, creating shallow mixed layers and increasing light levels in surface waters. Satellite ocean color observations suggest seasonal phytoplankton blooms occur over a third of the SIZ each spring (Fitch & Moore, 2007). The initiation of blooms in the SIZ has been attributed to an increase in light levels, sea ice melt induced surface stratification, sea ice algae release, and/or increased iron supply from melting ice following sea ice retreat (Ardyna et al., 2017; Selz et al., 2018; Smith & Comiso, 2008; Smith & Nelson, 1985).

The recent deployment of profiling floats equipped with biogeochemical sensors, primarily by the Southern Ocean Carbon and Climate Observations and Modeling project (SOCCOM; (Johnson, Plant, Coletti, et al., 2017)) has increased the capacity to study the SIZ through under-ice, multi-year, and basin-wide observations. Biogeochemical profiling float observations of chlorophyll fluorescence and particulate backscatter have recently indicated that the start of phytoplankton biomass accumulation begins between September and October, before sea ice melt detection and well before ice-free conditions in January and February (Arteaga et al., 2020; Hague & Vichi, 2021; Horvat et al., 2022; Uchida, Balwada, Abernathey, Prend, et al., 2019).

However, understanding the impact of SIZ phytoplankton blooms, especially under-ice, on mixed layer carbon and nutrient cycling, and their broader role in the total Southern Ocean carbon cycle has previously been limited by a lack of observations. Recent record minima in Antarctic sea ice extent and early sea ice retreats in 2017 and 2022 (Parkinson, 2019; Wang et al., 2022) underscore the need to understand the link between seasonal changes in sea ice cover and biological production in the Southern Ocean. Net community production (NCP) describes the fraction of primary production that is not respired in surface waters in contact with the atmosphere and can be exported into the ocean interior; NCP integrated over a full annual cycle is referred to as Annual NCP (ANCP). Estimates of SIZ NCP during the seasonal phytoplankton bloom (bNCP) from biogeochemical profiling floats indicate a wide range in total magnitude (1–3.5 mol C m^{-2} yr^{-1}), but analysis of bNCP in the SIZ has been limited to basin-scale averages or only a few floats (Arteaga et al., 2019; von Berg et al., 2020; Johnson, Plant, Dunne, et al., 2017). Here we link seasonal changes in phytoplankton biomass to NCP throughout the SIZ from 64 bloom observations from 2015 to 2021 to determine the link between sea ice cover, nutrient drawdown, and bNCP.

2. Methods

2.1. Data

Water column biogeochemical measurements of under-ice and recently ice-free waters are from SOCCOM profiling floats (Johnson, Plant, Coletti, et al., 2017). Processed and quality-controlled data are from float conductivity-temperature-depth, chlorophyll fluorescence, pH, particulate backscatter, nitrate, and oxygen sensors (Johnson, Plant, Coletti, et al., 2017; Maurer et al., 2021). SOCCOM-reported corrected chlorophyll concentrations ([Chl]) used in the analysis are derived from float fluorescence measurements corrected for non-photochemical quenching and a slope correction of 6 is applied based on observed Southern Ocean differences between high performance liquid chromatography and float-derived [Chl] (Johnson, et al., 2021). Phytoplankton carbon (C_p, mg C m^{-3}, Graff et al. (2015)) is inferred from float-measured particulate backscatter ($b_{bp(700)}$) (Morel & Maritorena, 2001):

$$b_{bp(470)} = b_{bp(700)} \times \left(\frac{470}{700}\right)^{-1} \quad (1)$$

$$[C_p] = 12128 \times b_{bp(470)} + 0.59 \quad (2)$$

For each float, data is interpolated to a uniform daily timestep and 1-dbar pressure grid. Daily interpolation of 10-day profile data eases comparison to daily data sets, but has inherent uncertainty as biological processes do not evolve linearly. However, conclusions do not change if 10-day differences are instead used. Mixed layer property means, mixed layer depth (MLD), and depth-integrated nitrate are smoothed with a 30-day running average. Nitrate is normalized to salinity to avoid sea ice melt biasing the seasonal changes in nitrate due to biological processes (Papadimitriou et al., 2012). Sea ice concentration (SIC) from NSIDC/NOAA Climate Data Record of Passive Microwave Sea Ice Concentration (Meier et al., 2021) and incident shortwave radiative flux from the ERA5 reanalysis (Hersbach et al., 2020) are matched to float positions, which are estimated through linear interpolation while floats are under-ice. SIC is used to determine the day of total sea ice retreat, defined as the first day of sea ice-free (SIC = 0%) conditions at the float location. MLD is calculated based on a potential density difference of 0.03 kg m^{-3} from either 10 m or the shallowest depth measured when the floats sense ice cover (~20 m), following de Boyer Montégut, (2004). Mixed layer median PAR (I_g) is estimated as in Westberry et al. (2008),

$$I_g = I_0 e^{-K_{\mathrm{PAR}} \cdot \frac{\mathrm{MLD}}{2}}, \quad (3)$$

where (K_{PAR}), the diffuse attenuation coefficient of photosynthetically active radiation (PAR), is estimated from Morel et al. (2007) (Text S1, Equations S2 and S3 in Supporting Information S1) and (I_0) is estimated from 2.3*incident shortwave radiative flux at the surface (Britton & Dodd, 1976). I_g is then adjusted for sea ice by linearly scaling with SIC using a 10% transmittance through the ice-covered fraction, based on available Southern Ocean transmittance observations (Castellani et al., 2020). We define a float season as data between July 1 and April 30 of each year. Float seasons are included in the analysis if the float was under-ice at least 30 consecutive days with SIC > 80% during winter and if both the winter nitrate maximum and spring nitrate minimum were observed. Float seasons with more than one consecutive missing profile for any variable are removed from analysis. In total, 64 seasons from 31 floats met the criteria between 2015 and 2021. Data is broadly distributed throughout the Southern Ocean between 58°S and 72°S (Figure 1, Table S1 in Supporting Information S1).

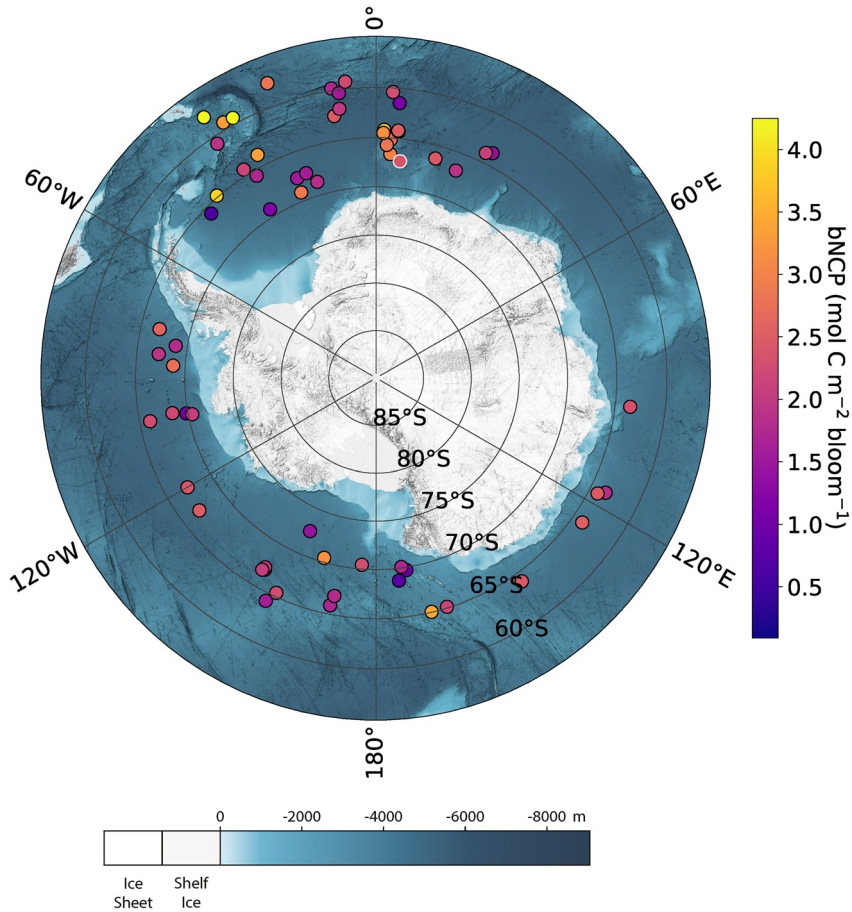

Figure 1. Mean float positions and bloom NCP. Ocean bathymetry (International Bathymetric chart of the Southern Ocean (IBSCO) version 2 (Dorschel et al., 2022)) overlayed with float positions at the time of the spring nitrate minimum (circles). Marker colors correspond to the magnitude of bNCP. Ice sheet and shelves are colored white/light gray, lighter blues correspond to shallower bathymetry including at Maud Rise (65°S, 3°E). Figures 2a and 2b float season is outlined in white.

2.2. Calculation of Growth Initiation/Tracer Timing Thresholds

To determine if changes in sea ice cover are associated with the onset of seasonal phytoplankton blooms and nutrient drawdown, we calculated phytoplankton growth initiation (GI) and compared when mean mixed layer nitrate, oxygen, and salinity, and SIC at the float location change from their winter values by a defined threshold (Equations 4–7), and continue to increase/decrease to their respective seasonal maxima/minima. GI_{Chl} and GI_{Cp} are estimated as the date mean mixed layer [Chl] or [Cp] first increase faster than the median rate of change while $\frac{d[Chl,Cp]}{dt} > 0$ for each float season, following previous work in the SIZ (Hague & Vichi, 2021). GI is chosen over bloom onset, which is typically defined when $\frac{d[Chl,Cp]}{dt} > 0$, because in winter $\frac{d[Chl,Cp]}{dt}$ can be >0 although [Cp]/[Chl] remain near remain zero and nitrate is increasing. Tracer change onsets are determined by:

$$\overline{[NO_3^-]}_{MLD} < \left(\overline{[NO_3^-]}_{MLD,winter\ max} - 0.2\ \mu mol\ kg^{-1}\right) \quad (4)$$

$$\overline{[O_2]}_{MLD} > \left(\overline{[O_2]}_{MLD,winter\ min} + \left(0.2\ \mu mol\ kg^{-1}\ NO_3^- \times 154\ O_2/17\ N\right)\right) \quad (5)$$

$$Salinity_{MLD} < \left(Salinity_{MLD,winter\ max} - 0.015\right) \quad (6)$$

$$SIC < \left(SIC_{winter\ max} - 2.5\%\right) \quad (7)$$

where winter maximum/minimum values are the mean of the two highest/lowest winter mixed layer values, and the nitrate threshold (Equation 4) is chosen to be sensitive to nitrate drawdown associated with GI, but exceed

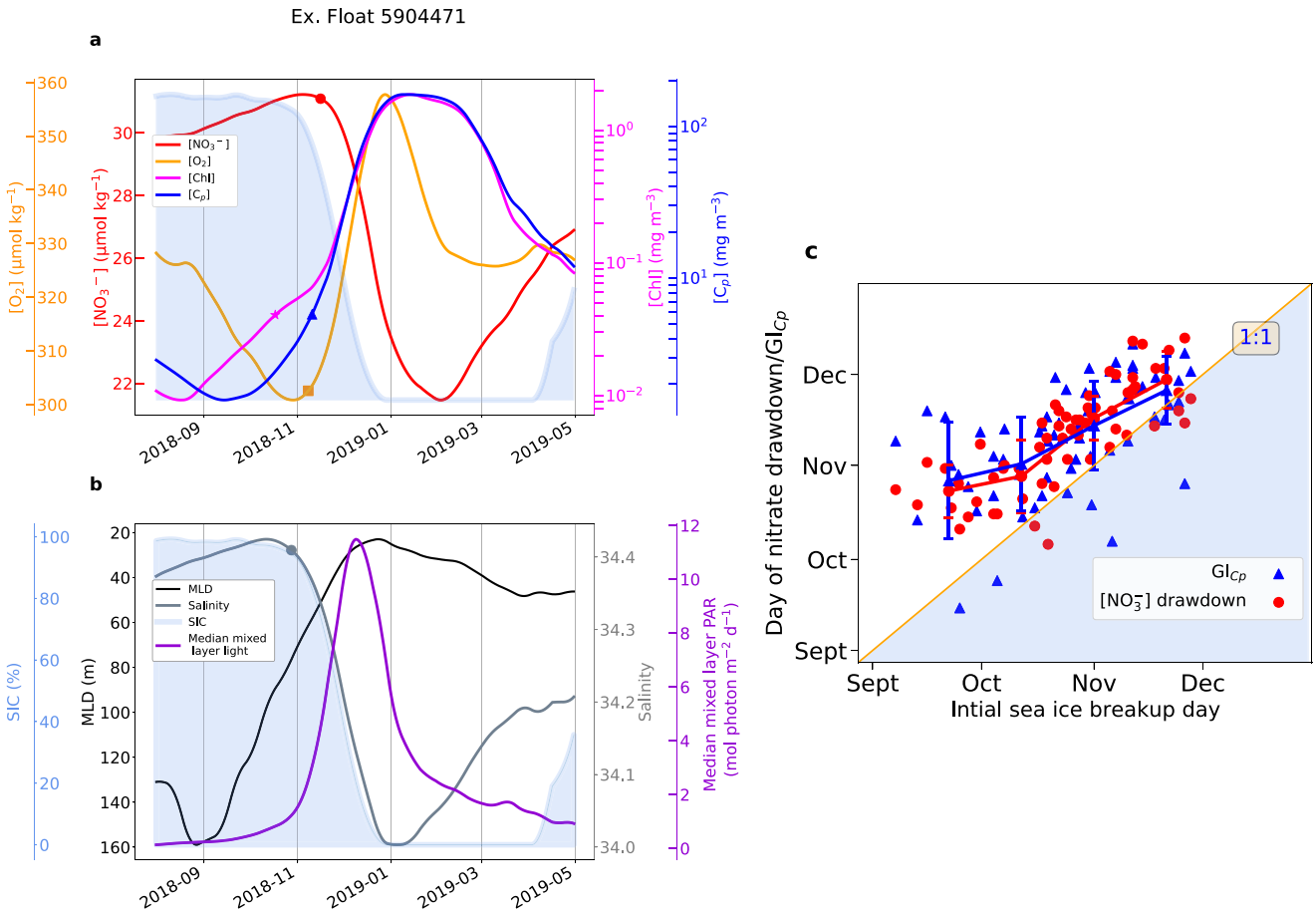

Figure 2. Seasonal relationships between mixed layer properties and SIC. Example float (WMO 5904471, white circle, Figure 1) season with mixed layer mean (a) oxygen (orange), nitrate (red), C_p (blue), and Chl (magenta) concentrations and (b) salinity (gray), MLD (black), and estimated PAR (purple). SIC is shaded blue for both (scale in b. only). Symbols indicate GI_{Chl}/GI_{Cp} or when nitrate, oxygen, or salinity thresholds are exceeded. (c) Nitrate drawdown onset (red circles) and GI_{Cp} (blue triangles) plotted against sea ice breakup day for all 64 float seasons analyzed. Red/blue error bars indicate 20-day bin means ±1 SD. Symbols above the gold 1:1 line (unshaded region) indicate sea ice breakup precedes mixed layer nitrate decrease and GI_{Cp}.

sensor noise (Text S2 in Supporting Information S1). The oxygen threshold (Equation 5) is set by multiplying the nitrate threshold by the −154/17 O_2/N ratio of photosynthesis/respiration (Hedges et al., 2002) so that biologically-driven oxygen increase onset coincides with nitrate drawdown onset. Oxygen increases prior to nitrate drawdown onset indicate air-sea exchange due to initial sea-ice breakup. The salinity threshold (Equation 6) was chosen to indicate mixed layer freshening that approximately corresponds to the SIC decrease threshold (Equation 7) based on the relationship between salinity and SIC during sea ice melt (Figure S1 in Supporting Information S1).

2.3. Net Community Production Estimates

We define bNCP as the cumulative NCP associated with the seasonal phytoplankton bloom. For each float season, bNCP is calculated from nitrate drawdown between the winter nitrate maximum and the summer nitrate minimum and converted to carbon units via a Redfield ratio of 6.6 C/N for the SIZ (Johnson et al., 2022). In order to estimate the amount of nitrate/carbon removed from the surface during the seasonal phytoplankton bloom that would not be re-entrained the following winter and to include sub-MLD NCP, we calculate nitrate drawdown from nitrate vertically integrated to the preceding deepest winter MLD. Changes in nitrate that result from advection or diffusion are not explicitly estimated due to difficulty in accurately parameterizing these fluxes under sea ice. However, we estimated the contribution from these processes to bNCP to be small compared to the magnitude of biological drawdown during this period using a state estimate (Text S3 in Supporting Information S1). NCP is determined from 10-day differences in float-measured nitrate. For ease of comparison, we present average daily

NCP from the 10-day differences. This choice does not change our results, as we compare relative NCP rates over ~50-day periods.

3. Results and Discussion

3.1. Timing of Changing Sea Ice Cover, Biomass Increase, and Nitrate Drawdown

From winter to summer for each float analyzed, mixed layer [C_p], [Chl], and [O_2] increase from their annual minima to maxima, and mixed layer [NO_3^-] and salinity decrease from annual maxima to minima (e.g., Figures 2a and 2b). The initial increase in mixed layer oxygen occurs before nitrate drawdown onset and coincides with the initial decrease in mixed layer salinity and SIC (Figures 2a and 2b). Decreases in salinity, decreases in SIC, and initial oxygen increase all differently indicate sea ice melt onset and the exposure of previously isolated water to atmospheric gases and increased light. We use an average of these three proxies to define initial sea ice breakup timing to minimize individual uncertainties (Text S2 in Supporting Information S1).

We compare estimates of GI, nitrate drawdown onset, and sea ice breakup for each float season and find that biological production closely follows the initial breakup of sea ice (Figure 2c). GI_{Cp} is coincident with nitrate drawdown (0 day difference ±13 days) and both almost always occur after sea ice breakup (GI_{Cp} occurs 17 ± 18 days after and nitrate drawdown onset occurs 17 ± 12 days after sea ice breakup). Sea ice breakup occurs as early as mid-September and as late as December. The lag between sea ice breakup and subsequent GI_{Cp} and nitrate drawdown is ~11 days longer when sea ice breakup occurs earlier (before mid-October, Figure 2c), than later (after mid-November).

In contrast, GI_{Chl} does not show a consistent relationship with GI_{Cp}, the onset of nitrate drawdown, or sea ice breakup, and often occurs before sea ice breakup (7 ± 23 days before sea ice breakup, Figure S2 in Supporting Information S1). However, there is no indication of biological production sufficient to influence surface nitrate and carbon concentrations prior to initial sea ice breakup, despite increases in chlorophyll weeks to months prior. When GI_{Chl} occurs early in the season and several months before initial sea ice breakup, both GI_{Cp} and nitrate drawdown onset still do not occur until after sea ice breakup and can lag GI_{Chl} by up to ~78 days (Figure S2 in Supporting Information S1). The difference between GI_{Cp} and GI_{Chl} is largely due to a high sensitivity of GI_{Chl} to very small changes in [Chl], which can be driven by photoacclimation rather than increasing phytoplankton biomass (Graff et al., 2016), and/or due to uncertainties in deriving [Chl] from float measured Chl-fluorescence (Boss & Haentjens, 2016). If we use a fixed 0.035 mg m^{-3} [Chl] threshold, based on the 0.2 µmol kg^{-1} [NO_3^-] threshold and a Chl:N ratio of 1.75 (Moreau et al., 2020), [Chl] increase timing is more similar to GI_{Cp} and nitrate drawdown onset (Figure S2 in Supporting Information S1). The discrepancy between GI_{Chl} and the [Chl] threshold approach highlights the advantage of assessing C_p and nitrate to characterize seasonal changes in phytoplankton biomass in the SIZ. Evidence that both GI_{Cp} and nitrate drawdown consistently follow initial sea ice breakup suggests that small openings in sea ice relieve light limitation and trigger under-ice biological production. Relief of light limitation through small openings in ice is consistent with studies showing increased phytoplankton biomass near leads in the Arctic (Assmy et al., 2017) and in-situ and model analysis of conditions to support under ice blooms in the Southern Ocean (Bisson & Cael, 2021; Horvat et al., 2022).

3.2. Seasonal Evolution of NCP Rates and Potential Drivers

After sea ice breakup, NCP rates rapidly increase as sea ice melts, coincident with increases in C_p (Figure S3 in Supporting Information S1). The highest NCP rates during the bloom occur before or soon after total sea ice retreat, shown by the slope of Figure 3a. Daily NCP rates are significantly lower during the open water period than under partial sea ice (Figure 3b, $p < 0.001$, details of statistical tests in Text S4 in Supporting Information S1). Taking the mean of all float seasons, 64 ± 18% of bNCP occurs under partial sea ice cover (Figure 3a). Iron limitation, grazing, and community composition may all interact to drive the observed decrease in daily NCP following total sea ice retreat. Although measurements of sea ice iron concentrations vary, iron in sea ice is an order of magnitude greater than in surface waters (Lannuzel et al., 2016) and field experiments show SIZ phytoplankton are strongly stimulated by additional iron (Alderkamp et al., 2019; Viljoen et al., 2018; Vives et al., 2022). Elevated dissolved iron concentrations during sea ice melt and a phytoplankton bloom have been observed in the SIZ, where both iron and phytoplankton concentrations declined after sea ice retreat (Croot et al., 2004), consistent with our observations of lower NCP rates after sea ice retreat.

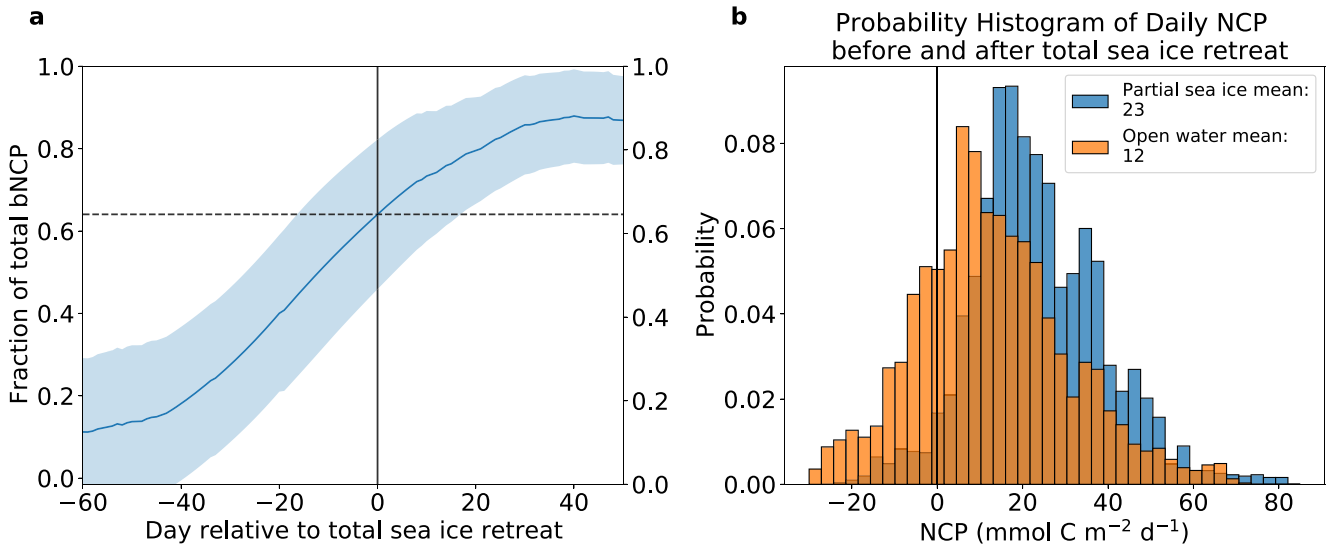

Figure 3. Relationship between NCP and sea ice cover. (a.) Mean cumulative fraction of total bNCP (solid line ±1 SD) with respect to time of total sea ice retreat (solid vertical line). Days on *x*-axis indicate time before or after total sea ice retreat. Horizontal dashed line indicates fraction of bNCP (mean of all float seasons) at mean day of total sea ice retreat. (b.) Probability histogram of daily NCP rates occurring 50 days before (blue) or after (orange) sea ice total sea ice retreat. Vertical line indicates zero NCP.

Shifts in phytoplankton community composition and/or increased grazing pressure may also decrease NCP rates after total sea ice retreat. Krill and salps are effective grazers of phytoplankton blooms following sea ice retreat and can significantly control NCP (Granĺi et al., 1993; Ishii et al., 2002; Lancelot et al., 1991; Mengesha et al., 1998). Furthermore, phytoplankton communities shift from *Phaeocystis* to diatom communities through the season in response to increasing iron limitation and temperature (Nissen & Vogt, 2021; Ryan-Keogh & Smith, 2021; Wright & Van den Enden, 2000) and krill selectively graze diatoms over *Phaeocystis* (Davidson et al., 2010; Haberman et al., 2003), which could cause higher grazing rates and contribute to observed lower NCP rates later in the season.

3.3. Bloom NCP Magnitude Variability

While the seasonality of NCP rates is similar between individual float seasons, the magnitude of bNCP ranges from <1 to >4 mol C m^{-2} bloom^{-1} (Figures 1 and 4a). In order to identify what factors influenced SIZ bNCP magnitude, we test the relationship between bNCP and timing of sea ice breakup, length of seasonal phytoplankton bloom (defined as the period over which bNCP is calculated), cumulative median mixed layer PAR from July to April, days with SIC < 15%, and duration of seasonally shallow (<40 m) MLD. Variability in bNCP magnitude is linearly related to the timing of sea ice breakup ($r^2 = 0.27$, $p < 0.001$), with higher bNCP found in regions or years with early sea ice breakup, defined as before mid-October (year day 290, 19 occurrences), and lower bNCP when sea ice breakup occurs later (Figure 4). On average, bNCP is 1 mol C m^{-2} bloom^{-1} higher for floats where sea ice retreats early (2.8 ± 0.9 mol C m^{-2} bloom^{-1}) rather than late (1.8 ± 0.8 mol C m^{-2} bloom^{-1}).

The number of days SIC < 15% is only weakly linearly related to the magnitude of bNCP ($r^2 = 0.118$, *P*-value = 0.005) (Figure S4 in Supporting Information S1), and the magnitude of bNCP is not significantly related to cumulative median mixed layer PAR, duration of nitrate drawdown, or duration of shallow mixed layers. These results indicate higher available light over longer periods of time are not responsible for higher bNCP. Similarly, differences between early and late sea ice breakup bNCP cannot be explained by seasonal differences in available light; floats that observe early sea ice breakup have lower light availability and higher daily NCP rates compared with floats that observe late sea ice breakup (Figure 4b). While PAR estimates are uncertain (Text S1 in Supporting Information S1), the lack of correlation between bNCP and factors that increase light in the mixed layer indicate that after light limitation is relieved by sea ice breakup, factors other than light availability control the magnitude of SIZ bNCP.

Floats that capture early sea ice retreat also observe significantly higher daily NCP rates and higher mixed layer [C_p] than floats that observed late sea ice breakup ($p < 0.001$) (Figure 4b, Figure S5 in Supporting Information S1).

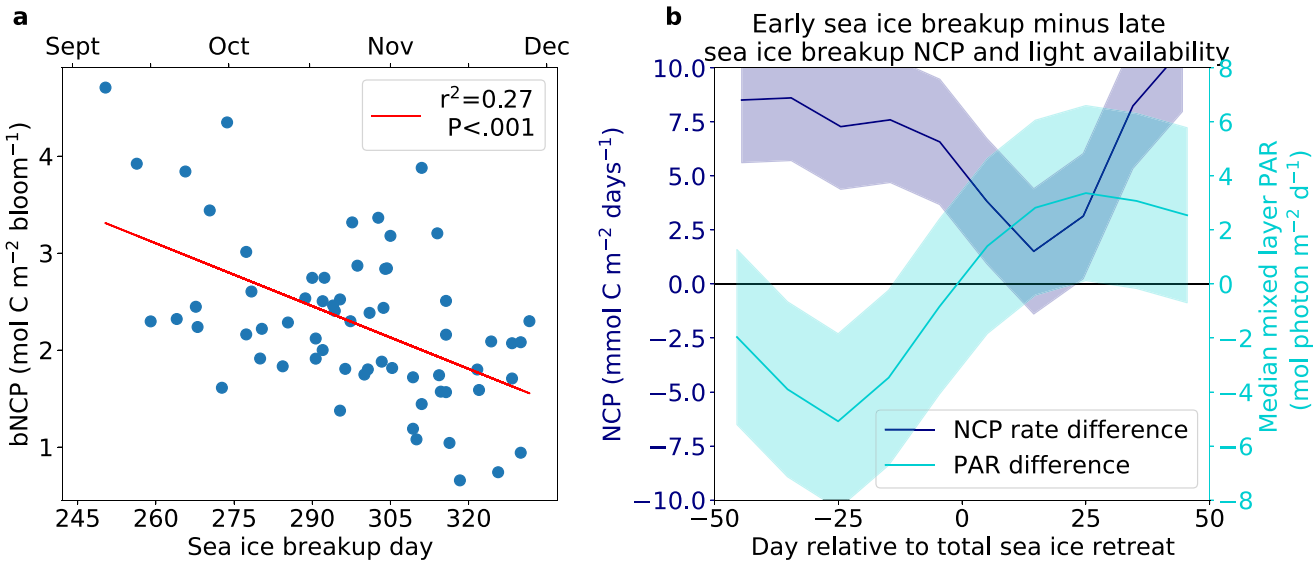

Figure 4. Relationship between NCP and timing of sea ice breakup. (a) bNCP is negatively correlated (red line, $p < 0.001$) with sea ice breakup date. (b) Difference in mean daily NCP (purple line) and mixed layer median PAR (blue line) between early sea ice breakup group (before year day 290) and late sea ice breakup group (after year day 310) versus day relative to total sea ice retreat day. Both daily NCP and mixed layer median PAR are 10-day binned means of all float seasons in each group.

We postulate that high bNCP associated with early sea ice breakup could be due to a greater lag between initial phytoplankton biomass increases and grazer (predominately krill) response when sea ice breaks up earlier in the year. Seasonal increases in grazers typically follow phytoplankton increase; however, certain taxa respond slowly to phytoplankton phenological shifts associated with earlier sea ice breakup, which could lead to trophic mismatches (Conroy et al., 2023). Krill also migrate southward with the sea ice edge, which could lead to higher grazing pressures in regions where sea ice breakup occurs later in the season (Brierley et al., 2022; Loeb & Santora, 2015). However, more research throughout the SIZ is needed to identify how changes in sea ice affect trophic dynamics.

The five highest bNCP estimates (3.8–4.7 mol C m^{-2} $bloom^{-1}$) occur in two regions with potentially elevated iron supply: near Maud Rise and near islands in the north-western Weddell Sea (Figure 1). Near Maud rise, flow topography interactions can enhance upwelling of deep waters (Mohrmann et al., 2022), and this topographically-induced mixing could supply iron from depth to support the high bNCP values. Both models and available in-situ dissolved iron data also show relatively high concentrations near the north-western Weddell Sea islands (Laufkötter et al., 2018; Person et al., 2021; Tagliabue et al., 2012).

Some of the variability in bNCP may be explained by regional differences in iron supply from icebergs, glacial melt, and sea ice, as well as from winter mixing and eddies, which support Southern Ocean phytoplankton blooms in northern regions (Llort et al., 2002; Rosso et al., 2016; Sallée et al., 2015; Uchida, Balwada, Abernathey, McKinley, et al., 2019; Uchida et al., 2020). However, resolving SIZ iron sources and iron limitation is currently difficult due to sparse observations during the winter-spring transition (Tagliabue et al., 2012). New proxies for iron limitation developed in the Southern Ocean (Ryan-Keogh & Smith, 2021; Schallenberg et al., 2022), the addition of radiometers to under-ice floats, and increased observations of iron concentrations could support investigation of spatiotemporal patterns of iron limitation throughout the SIZ.

3.4. Relevance to Satellite Derived Estimates of Production

Positive NCP occurs well before the 10% SIC threshold used to identify ice-covered areas in previous work assessing SIZ blooms from satellite ocean color products (e.g., Ardyna et al. (2017); Arrigo et al. (2008)). Estimates of ANCP or carbon export in the SIZ that use NPP derived from satellite ocean color are limited to spring/summer due to seasonal lack of light and ice cover the rest of the year and therefore can be compared to our bNCP estimates. Satellite-derived ANCP estimates (~1–1.5 mol C m^{-2} yr^{-1} (Arteaga et al., 2018; Li et al., 2021)) are on the lowest end of bNCP estimated from the floats (<1 to >4 mol C m^{-2} yr^{-1}). As the majority of bNCP occurs

before sea ice retreat is complete, the SIZ may contribute more to Southern Ocean NCP than previously estimated from satellite observations. NPP estimates that include modeled under-ice blooms suggest a higher marginal ice zone (MIZ, a subset of the SIZ around the sea ice edge) contribution to total Southern Ocean NPP south of 30°S (15%) than estimates from satellite ocean color observations (~4%) (Arrigo et al., 2008; Moore & Abbott, 2000; Taylor et al., 2013). Taylor et al. (2013) found blooms initiated when SIC fell below 90% and under-ice NPP accounted for two thirds of the NPP in the MIZ, which is within the uncertainty of our estimates of the fraction of bNCP under ice. Similarly, in the Southern Ocean south of 50°S, estimates of carbon export derived from inverse modeling and spring/summer climatological nitrate budgets are higher than satellite-derived estimates, which could partially be explained by under-ice carbon export (Maccready & Quay, 2001; Schlitzer, 2002). However, bNCP does not account for fall/wintertime respiration of organic carbon in surface waters and ANCP should be assessed in future work. ANCP estimated from one SIZ float indicated a near balance between bNCP and subsequent winter remineralization (Briggs et al., 2018).

4. Conclusions

Our results indicate that initial sea ice breakup triggers biological production and positive NCP under high sea ice cover and considerably before satellite ocean color observations can be leveraged. This provides the first in situ evidence of the biogeochemical importance of under-ice blooms and suggests that the SIZ may contribute more to total Southern Ocean NCP than previously estimated. The majority of bNCP occurs as sea ice is actively melting, and NCP rates are lower after sea ice retreat, possibly due to seasonal changes in micronutrient availability, phytoplankton community composition, and/or grazing pressure. The magnitude of bNCP is related to the timing of sea ice breakup, indicating that future changes in sea ice may change the timing and magnitude of seasonal blooms and bNCP.

Data Availability Statement

Profiling float data were collected and made freely available by the Southern Ocean Carbon and Climate Observations and Modeling (SOCCOM) Project funded by the National Science Foundation, Division of Polar Programs (NSF PLR-1425989 and OPP-1936222), supplemented by NASA, and by the International Argo Program and the NOAA programs that contribute to it (http://www.argo.ucsd.edu/, http://argo.jcommops.org/). The Argo Program is part of the Global Ocean Observing System. The May 2021 quarterly snapshot data set is used in this analysis and is available at doi.org/10.6075/J0T43SZG. Mean surface downward short-wave radiation flux was downloaded from the Copernicus Climate Change Service (C3S) Climate Data Store https://doi.org/10.24381/cds.f17050d7 (Hersbach et al., 2020). The results contain modified Copernicus Climate Change Service information 2020. Neither the European Commission nor ECMWF is responsible for any use that may be made of the Copernicus information or data it contains. NOAA/NSIDC Climate Data Record of Passive Microwave Sea Ice Concentration, Version 4 (G02202) is available for download at https://doi.org/10.7265/efmz-2t65. The International Bathymetric Chart of the Southern Ocean v2 digital bathymetric model is available for download at https://doi.org/10.1594/PANGAEA.937574. Code used for the analysis is available for download at https://doi.org/10.5281/zenodo.7192129.

Acknowledgments
S. McClish was supported by a Future Investigators in NASA Earth and Space Science and Technology award (80NSSC21K1641) and NASA-NNX17AI73G. S. Bushinsky was supported by NASA (NNX17AI73G, 80NSSC22K0156), NOAA-NA21OAR4310260, and NSF OCE-2049631. SOEST contribution #11727.

References

Alderkamp, A. C., van Dijken, G. L., Lowry, K. E., Lewis, K. M., Joy-Warren, H. L., van de Poll, W., et al. (2019). Effects of iron and light availability on phytoplankton photosynthetic properties in the Ross Sea. *Marine Ecology Progress Series*, *621*, 33–50. https://doi.org/10.3354/meps13000

Ardyna, M., Claustre, H., Sallée, J. B., D'Ovidio, F., Gentili, B., van Dijken, G., et al. (2017). Delineating environmental control of phytoplankton biomass and phenology in the Southern Ocean. *Geophysical Research Letters*, *44*(10), 5016–5024. https://doi.org/10.1002/2016GL072428

Arrigo, K. R., van Dijken, G. L., & Bushinsky, S. (2008). Primary production in the Southern Ocean, 1997-2006. *Journal of Geophysical Research*, *113*(C8), C08004. https://doi.org/10.1029/2007JC004551

Arteaga, L., Haëntjens, N., Boss, E., Johnson, K. S., & Sarmiento, J. L. (2018). Assessment of export efficiency equations in the southern ocean applied to satellite-based net primary production. *Journal of Geophysical Research: Oceans*, *123*(4), 2945–2964. https://doi.org/10.1002/2018JC013787

Arteaga, L. A., Boss, E., Behrenfeld, M. J., Westberry, T. K., & Sarmiento, J. L. (2020). Seasonal modulation of phytoplankton biomass in the southern ocean. *Nature Communications*, *11*(1), 5364. https://doi.org/10.1038/s41467-020-19157-2

Arteaga, L. A., Pahlow, M., Bushinsky, S. M., & Sarmiento, J. L. (2019). Nutrient controls on export production in the southern ocean. *Global Biogeochemical Cycles*, *33*(8), 942–956. https://doi.org/10.1029/2019GB006236

Assmy, P., Fernández-Méndez, M., Duarte, P., Meyer, A., Randelhoff, A., Mundy, C. J., et al. (2017). Leads in Arctic pack ice enable early phytoplankton blooms below snow-covered sea ice. *Scientific Reports*, *7*, 1–9. https://doi.org/10.1038/srep40850

Bisson, K. M., & Cael, B. B. (2021). How are under ice phytoplankton related to sea ice in the southern ocean? *Geophysical Research Letters*, *48*(21), 1–9. https://doi.org/10.1029/2021gl095051

Boss, E. B., & Haentjens, N. (2016). Primer regarding measurements of chlorophyll fluorescence and the backscattering coefficient with WETLabs FLBB on profiling floatsTechnical Report 2016-1. Retrieved from http://soccom.princeton.edu/sites/default/files/files/SOCCOM_2016-1_Bio-optics-primer.pdf

Brierley, A. S., Fernandes, P. G., Brandon, M. A., Armstrong, F., Millard, N. W., McPhail, S. D., et al. (2022). Antarctic krill under sea ice: Elevated abundance in a narrow band just south of ice edge. 13. In G. R. Sarson (Ed.), *Philos. Trans. R. Soc. London Ser. A* (Vol. 24). Academic Press. Retrieved from https://www.science.org

Briggs, E. M., Martz, T. R., Talley, L. D., Mazloff, M. R., & Johnson, K. S. (2018). Physical and biological drivers of biogeochemical tracers within the seasonal sea ice zone of the southern ocean from profiling floats. *Journal of Geophysical Research: Oceans*, *123*(2), 746–758. https://doi.org/10.1002/2017JC012846

Britton, C. M., & Dodd, J. D. (1976). Relationships of photosynthetically active radiation and shortwave irradiance. *Agricultural Meteorology*, *17*(1), 1–7. https://doi.org/10.1016/0002-1571(76)90080-7

Castellani, G., Schaafsma, F. L., Arndt, S., Lange, B. A., Peeken, I., Ehrlich, J., et al. (2020). Large-scale variability of physical and biological sea-ice properties in polar oceans. *Frontiers in Marine Science*, *7*, 1–22. https://doi.org/10.3389/fmars.2020.00536

Conroy, J., Steinberg, D., Thomas, M., & West, L. (2023). Seasonal and interannual changes in a coastal Antarctic zooplankton community. *Marine Ecology Progress Series*, *706*, 17–32. https://doi.org/10.3354/meps14256

Croot, P. L., Andersson, K., Öztürk, M., & Turner, D. R. (2004). The distribution and speciation of iron along 6°E in the Southern Ocean. *Deep-Sea Research Part II Topical Studies in Oceanography*, *51*(22–24), 2857–2879. https://doi.org/10.1016/j.dsr2.2003.10.012

Davidson, A. T., Scott, F. J., Nash, G. V., Wright, S. W., & Raymond, B. (2010). Physical and biological control of protistan community composition, distribution and abundance in the seasonal ice zone of the Southern Ocean between 30 and 80°E. *Deep-Sea Research Part II Topical Studies in Oceanography*, *57*(9–10), 828–848. https://doi.org/10.1016/j.dsr2.2009.02.011

de Boyer Montégut, C. (2004). Mixed layer depth over the global ocean: An examination of profile data and a profile-based climatology. *Journal of Geophysical Research*, *109*(C12), C12003. https://doi.org/10.1029/2004JC002378

Dorschel, B., Hehemann, L., Viquerat, S., Warnke, F., Dreutter, S., Tenberge, Y. S., et al. (2022). The international bathymetric chart of the southern ocean version 2. *Scientific Data*, *9*(1), 275. https://doi.org/10.1038/s41597-022-01366-7

Fitch, D. T., & Moore, J. K. (2007). Wind speed influence on phytoplankton bloom dynamics in the Southern Ocean marginal ice zone. *Journal of Geophysical Research*, *112*(8), 1–13. https://doi.org/10.1029/2006JC004061

Graff, J. R., Westberry, T. K., Milligan, A. J., Brown, M. B., Dall'Olmo, G., Reifel, K. M., & Behrenfeld, M. J. (2016). Photoacclimation of natural phytoplankton communities. *Marine Ecology Progress Series*, *542*, 51–62. https://doi.org/10.3354/meps11539

Graff, J. R., Westberry, T. K., Milligan, A. J., Brown, M. B., Dall'Olmo, G., van Dongen-Vogels, V., et al. (2015). Analytical phytoplankton carbon measurements spanning diverse ecosystems. *Deep-Sea Research Part I Oceanographic Research Papers*, *102*, 16–25. https://doi.org/10.1016/j.dsr.2015.04.006

Granĺi, E., Granéli, W., Rabbani, M. M., Daugbjerg, N., Fransz, G., Roudy, J. C., & Alder, V. A. (1993). The influence of copepod and krill grazing on the species composition of phytoplankton communities from the Scotia Weddell Sea - An experimental approach. *Polar Biology*, *13*(3), 201–213. https://doi.org/10.1007/BF00238930

Haberman, K. L., Quetin, L. B., & Ross, R. M. (2003). Diet of the Antarctic krill (Euphausia superba Dana): I. Comparisons of grazing on Phaeocystis Antarctica (Karsten) and Thalassiosira Antarctica (Comber). *Journal of Experimental Marine Biology and Ecology*, *283*(1–2), 79–95. https://doi.org/10.1016/S0022-0981(02)00466-5

Hague, M., & Vichi, M. (2021). Southern ocean biogeochemical Argo detect under-ice phytoplankton growth before sea ice retreat. *Biogeosciences*, *18*(1), 25–38. https://doi.org/10.5194/bg-18-25-2021

Hedges, J. I., Baldock, J. A., Gélinas, Y., Lee, C., Peterson, M. L., & Wakeham, S. G. (2002). The biochemical and elemental compositions of marine plankton: A NMR perspective (pp. 47–63). https://doi.org/10.1016/S0304-4203(02)00009-9

Hersbach, H., Bell, B., Berrisford, P., Hirahara, S., Horányi, A., Muñoz-Sabater, J., et al. (2020). The ERA5 global reanalysis. *Quarterly Journal of the Royal Meteorological Society*, *146*(730), 1999–2049. https://doi.org/10.1002/qj.3803

Horvat, C., Bisson, K., Seabrook, S., Cristi, A., & Matthes, L. C. (2022). Evidence of phytoplankton blooms under Antarctic sea ice. *Frontiers in Marine Science*, *9*. https://doi.org/10.3389/fmars.2022.942799

Ishii, M., Inoue, H. Y., & Matsueda, H. (2002). Net community production in the marginal ice zone and its importance for the variability of the oceanic pCO_2 in the Southern Ocean south of Australia. *Deep Sea Research Part II: Topical Studies in Oceanography*, *49*(9–10), 1691–1706. https://doi.org/10.1016/S0967-0645(02)00007-3

Johnson, K. S., Mazloff, M. R., Bif, M. B., Takeshita, Y., Jannasch, H. W., Maurer, T. L., et al. (2022). Carbon to nitrogen uptake ratios observed across the Southern Ocean by the SOCCOM profiling float array. *Journal of Geophysical Research: Oceans*, *127*(9), e2022JC018859. https://doi.org/10.1029/2022jc018859

Johnson, K. S., Plant, J. N., Coletti, L. J., Jannasch, H. W., Sakamoto, C. M., Riser, S. C., et al. (2017). Biogeochemical sensor performance in the SOCCOM profiling float array. *Journal of Geophysical Research: Oceans*, *122*(8), 6416–6436. https://doi.org/10.1002/2017JC012838

Johnson, K. S., Plant, J. N., Dunne, J. P., Talley, L. D., & Sarmiento, J. L. (2017). Annual nitrate drawdown observed by SOCCOM profiling floats and the relationship to annual net community production. *Journal of Geophysical Research: Oceans*, *122*(8), 6668–6683. https://doi.org/10.1002/2017JC012839

Johnson, K. S., Riser, S. C., Boss, E. S., Talley, L. D., Sarmiento, J. L., Swift, D. D., et al. (2021). SOCCOM float data - Snapshot 2021-05-05. In *Southern ocean carbon and climate observations and modeling (SOCCOM) float data archive*. UC San Diego Library Digital Collections. https://doi.org/10.6075/J0T43SZG

Lancelot, C., Billen, G., Veth, C., Becquevort, S., & Mathot, S. (1991). Modelling carbon cycling through phytoplankton and microbes in the Scotia—Weddell Sea area during sea ice retreat. *Marine Chemistry*, *35*(1–4), 305–324. https://doi.org/10.1016/S0304-4203(09)90024-X

Lannuzel, D., Vancoppenolle, M., van der Merwe, P., de Jong, J., Meiners, K. M., Nishioka, et al. (2016). Iron in sea ice: Review and new insights. https://doi.org/10.12952/journal.elementa.000130

Laufkötter, C., Stern, A. A., John, J. G., Stock, C. A., & Dunne, J. P. (2018). Glacial iron sources stimulate the southern ocean carbon cycle. *Geophysical Research Letters*, *45*(24), 13377–13385. https://doi.org/10.1029/2018GL079797

Li, Z., Lozier, M. S., & Cassar, N. (2021). Linking southern ocean mixed-layer dynamics to net community production on various timescales. *Journal of Geophysical Research: Oceans*, *126*(10), 1–14. https://doi.org/10.1029/2021JC017537

Llort, J., Lévy, M., Sallée, J.-B., & Tagliabue, A. (2002). Onset, intensification, and decline of phytoplankton blooms in the Southern Ocean. *The American Biology Teacher*, *64*(5), 382–383. https://doi.org/10.2307/4451315

Loeb, V. J., & Santora, J. A. (2015). Climate variability and spatiotemporal dynamics of five Southern Ocean krill species. *Progress in Oceanography*, *134*, 93–122. https://doi.org/10.1016/j.pocean.2015.01.002

Maccready, P., & Quay, P. (2001). Biological export flux in the Southern Ocean estimated from a climatological nitrate budget. *Deep-Sea Research II*, *48*(19–20), 4299–4322. https://doi.org/10.1016/s0967-0645(01)00090-x

Maurer, T. L., Plant, J. N., & Johnson, K. S. (2021). Delayed-mode quality control of oxygen, nitrate, and pH data on SOCCOM biogeochemical profiling floats. *Frontiers in Marine Science*, *8*. https://doi.org/10.3389/fmars.2021.683207

Meier, W. N., Peng, G., Scott, D. J., & Savoie, M. H. (2021). *NOAA/NSIDC climate data record of passive microwave sea ice concentration, Version 4*. National Snow and Ice Data Center.

Mengesha, S., Dehairs, F., Fiala, M., Elskens, M., & Goeyens, L. (1998). Seasonal variation of phytoplankton community structure and nitrogen uptake regime in the Indian Sector of the Southern Ocean. *Polar Biology*, *20*(4), 259–272. https://doi.org/10.1007/s003000050302

Mohrmann, M., Swart, S., & Heuzé, C. (2022). Observed mixing at the flanks of Maud rise in the Weddell Sea. *Geophysical Research Letters*, *49*(8), e2022GL098036. https://doi.org/10.1029/2022GL098036

Moore, J. K., & Abbott, M. R. (2000). Phytoplankton chlorophyll distributions and primary production in the Southern Ocean. *Journal of Geophysical Research*, *105*(C12), 28709–28722. https://doi.org/10.1029/1999jc000043

Moreau, S., Boyd, P. W., & Strutton, P. G. (2020). Remote assessment of the fate of phytoplankton in the Southern Ocean sea-ice zone. *Nature Communications*, *11*(1), 3108. https://doi.org/10.1038/s41467-020-16931-0

Morel, A., Huot, Y., Gentili, B., Werdell, P. J., Hooker, S. B., & Franz, B. A. (2007). Examining the consistency of products derived from various ocean color sensors in open ocean (Case 1) waters in the perspective of a multi-sensor approach. *Remote Sensing of Environment*, *111*(1), 69–88. https://doi.org/10.1016/j.rse.2007.03.012

Morel, A., & Maritorena, S. (2001). Bio-optical properties of oceanic waters: A reappraisal. *Journal of Geophysical Research*, *106*(C4), 7163–7180. https://doi.org/10.1029/2000jc000319

Nissen, C., & Vogt, M. (2021). Factors controlling the competition between *Phaeocystis* and diatoms in the Southern Ocean and implications for carbon export fluxes. *Biogeosciences*, *18*(1), 251–283. https://doi.org/10.5194/bg-18-251-2021

Papadimitriou, S., Kennedy, H., Norman, L., Kennedy, D. P., Dieckmann, G. S., & Thomas, D. N. (2012). The effect of biological activity, $CaCO_3$ mineral dynamics, and CO_2 degassing in the inorganic carbon cycle in sea ice in late winter-early spring in the Weddell Sea, Antarctica. *Journal of Geophysical Research*, *117*(8), 1–12. https://doi.org/10.1029/2012JC008058

Parkinson, C. L. (2019). A 40-y record reveals gradual Antarctic sea ice increases followed by decreases at rates far exceeding the rates seen in the Arctic. *Proceedings of the National Academy of Sciences of the United States of America*, *116*(29), 14414–14423. https://doi.org/10.1073/pnas.1906556116

Pellichero, V., Sallée, J.-B., Schmidtko, S., Roquet, F., & Charrassin, J.-B. (2017). The ocean mixed layer under southern ocean sea-ice: Seasonal cycle and forcing. *Journal of Geophysical Research: Oceans*, *122*(2), 1608–1633. https://doi.org/10.1002/2016JC011970

Person, R., Vancoppenolle, M., Aumont, O., & Malsang, M. (2021). Continental and sea ice iron sources fertilize the southern ocean in synergy. *Geophysical Research Letters*, *48*(23), 1–9. https://doi.org/10.1029/2021GL094761

Rosso, I., Hogg, A. M., Matear, R., & Strutton, P. G. (2016). Quantifying the influence of sub-mesoscale dynamics on the supply of iron to Southern Ocean phytoplankton blooms. *Deep Sea Research Part I: Oceanographic Research Papers*, *115*, 199–209. https://doi.org/10.1016/j.dsr.2016.06.009

Ryan-Keogh, T. J., & Smith, W. O. (2021). Temporal patterns of iron limitation in the Ross Sea as determined from chlorophyll fluorescence. *Journal of Marine Systems*, *215*, 103500. https://doi.org/10.1016/j.jmarsys.2020.103500

Sallée, J. B., Llort, J., Tagliabue, A., & Lévy, M. (2015). Characterization of distinct bloom phenology regimes in the Southern Ocean. *ICES Journal of Marine Science*, *72*(6), 1985–1998. https://doi.org/10.1093/icesjms/fsv069

Schallenberg, C., Strzepek, R. F., Bestley, S., Bozena, W., & Trull, T. W. (2022). Iron limitation drives the globally extreme Fluorescence/Chlorophyll ratios of the Southern Ocean. *Geophysical Research Letters*, *49*(12), e2021GL097616. https://doi.org/10.1029/2021GL097616

Schlitzer, R. (2002). Carbon export fluxes in the southern ocean: Results from inverse modeling and comparison with satellite-based estimates. *Deep-Sea Research Part II Topical Studies in Oceanography*, *49*(9–10), 1623–1644. https://doi.org/10.1016/S0967-0645(02)00004-8

Selz, V., Lowry, K. E., Lewis, K. M., Joy-Warren, H. L., van de Poll, W., Nirmel, S., et al. (2018). Distribution of Phaeocystis Antarctica-dominated sea ice algal communities and their potential to seed phytoplankton across the western Antarctic Peninsula in spring. *Marine Ecology Progress Series*, *586*, 91–112. https://doi.org/10.3354/meps12367

Smith, W. O., & Comiso, J. C. (2008). Influence of sea ice on primary production in the Southern Ocean: A satellite perspective. *Journal of Geophysical Research*, *113*(5), 1–19. https://doi.org/10.1029/2007JC004251

Smith, W. O., & Nelson, D. M. (1985). Phytoplankton bloom produced by a receding ice edge in the Ross Sea: Spatial coherence with the density field. *Science*, *227*(4683), 163–166. https://doi.org/10.1126/science.227.4683.163

Tagliabue, A., Mtshali, T., Aumont, O., Bowie, A. R., Klunder, M. B., Roychoudhury, A. N., & Swart, S. (2012). A global compilation of dissolved iron measurements: Focus on distributions and processes in the Southern Ocean. *Biogeosciences*, *9*(6), 2333–2349. https://doi.org/10.5194/bg-9-2333-2012

Taylor, M. H., Losch, M., & Bracher, A. (2013). On the drivers of phytoplankton blooms in the Antarctic marginal ice zone: A modeling approach. *Journal of Geophysical Research: Oceans*, *118*(1), 63–75. https://doi.org/10.1029/2012JC008418

Uchida, T., Balwada, D., Abernathey, R., McKinley, G., Smith, S., & Levy, M. (2019). The contribution of submesoscale over mesoscale eddy iron transport in the open Southern Ocean. *Journal of Advances in Modeling Earth Systems*, *11*(12), 3934–3958. https://doi.org/10.1029/2019MS001805

Uchida, T., Balwada, D., Abernathey, R., Prend, C. J., Boss, E., & Gille, S. T. (2019). Southern ocean phytoplankton blooms observed by biogeochemical floats. *Journal of Geophysical Research: Oceans*, *124*(11), 7328–7343. https://doi.org/10.1029/2019JC015355

Uchida, T., Balwada, D., Abernathey, R. P., McKinley, G. A., Smith, S. K., & Lévy, M. (2020). Vertical eddy iron fluxes support primary production in the open Southern Ocean. *Nature Communications*, *11*(1), 1125. https://doi.org/10.1038/s41467-020-14955-0

Viljoen, J. J., Philibert, R., van Horsten, N., Mtshali, T., Roychoudhury, A. N., Thomalla, S., & Fietz, S. (2018). Phytoplankton response in growth, photophysiology and community structure to iron and light in the Polar Frontal Zone and Antarctic waters. *Deep-Sea Research Part I Oceanographic Research Papers*, *141*, 118–129. https://doi.org/10.1016/j.dsr.2018.09.006

Vives, C. R., Schallenberg, C., Strutton, P. G., & Westwood, K. J. (2022). Iron and light limitation of phytoplankton growth off East Antarctica. *Journal of Marine Systems*, *234*, 103774. https://doi.org/10.1016/j.jmarsys.2022.103774

von Berg, L., Prend, C. J., Campbell, E. C., Mazloff, M. R., Talley, L. D., & Gille, S. T. (2020). Weddell sea phytoplankton blooms modulated by sea ice variability and polynya formation. *Geophysical Research Letters*, *47*(11), 1–12. https://doi.org/10.1029/2020GL087954

Wang, J., Luo, H., Yang, Q., Liu, J., Yu, L., Shi, Q., & Han, B. (2022). An unprecedented record low Antarctic sea-ice extent during Austral Summer 2022. *Advances in Atmospheric Sciences*, *39*(10), 1591–1597. https://doi.org/10.1007/s00376-022-2087-1

Westberry, T., Behrenfeld, M. J., Siegel, D. A., & Boss, E. (2008). Carbon-based primary productivity modeling with vertically resolved photoacclimation. *Global Biogeochemical Cycles*, *22*(2), GB2024. https://doi.org/10.1029/2007GB003078

Wright, S. W., & van den Enden, R. L. (2000). Phytoplankton community structure and stocks in the East Antarctic marginal ice zone (BROKE survey, January-March 1996) determined by CHEMTAX analysis of HPLC pigment signatures. *Deep-Sea Research Part II Topical Studies in Oceanography*, *47*(12–13), 2363–2400. https://doi.org/10.1016/S0967-0645(00)00029-1

References From the Supporting Information

Giddy, I., Swart, S., Du Plessis, M., Thompson, A. F., & Nicholson, S. A. (2021). Stirring of sea-ice meltwater enhances submesoscale fronts in the southern ocean. *Journal of Geophysical Research: Oceans*, *126*(4), e2020JC016814. https://doi.org/10.1029/2020JC016814

Lin, Y., Moreno, C., Marchetti, A., Ducklow, H., Schofield, O., Delage, E., et al. (2021). Decline in plankton diversity and carbon flux with reduced sea ice extent along the Western Antarctic Peninsula. *Nature Communications*, *12*(1), 1–9. https://doi.org/10.1038/s41467-021-25235-w

Manucharyan, G. E., & Thompson, A. F. (2017). Submesoscale sea ice-ocean interactions in marginal ice zones. *Journal of Geophysical Research: Oceans*, *122*(12), 9455–9475. https://doi.org/10.1002/2017JC012895